A new bismuth coordination polymer with proton conductivity and orange-red photoluminescence

Aliyu M. Hamisu

Journal of coordination chemistry

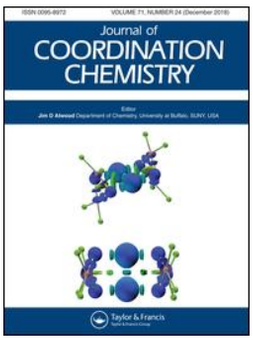

Taylor & Francis
Taylor & Francis Group

Journal of Coordination Chemistry

ISSN: (Print) (Online) Journal homepage: https://www.tandfonline.com/loi/gcoo20

A new bismuth coordination polymer with proton conductivity and orange-red photoluminescence

Mesoun A. A. Al-Nubi, Aliyu M. Hamisu, Azhar Ariffin, Jinfeng Zhang, George K. H. Shimizu, Hongil Jo, Kang Min Ok & Arief C. Wibowo

To cite this article: Mesoun A. A. Al-Nubi, Aliyu M. Hamisu, Azhar Ariffin, Jinfeng Zhang, George K. H. Shimizu, Hongil Jo, Kang Min Ok & Arief C. Wibowo (2021): A new bismuth coordination polymer with proton conductivity and orange-red photoluminescence, Journal of Coordination Chemistry, DOI: 10.1080/00958972.2021.1921167

To link to this article: https://doi.org/10.1080/00958972.2021.1921167

JOURNAL OF COORDINATION CHEMISTRY
https://doi.org/10.1080/00958972.2021.1921167

Taylor & Francis
Taylor & Francis Group

A new bismuth coordination polymer with proton conductivity and orange-red photoluminescence

Mesoun A. A. Al-Nubi[a], Aliyu M. Hamisu[a], Azhar Ariffin[a], Jinfeng Zhang[b], George K. H. Shimizu[b], Hongil Jo[c], Kang Min Ok[c] and Arief C. Wibowo[d]

[a]Department of Chemistry, University of Malaya, Kuala Lumpur, Malaysia; [b]Department of Chemistry, University of Calgary, Alberta, Canada; [c]Department of Chemistry, Sogang University, Seoul, South Korea; [d]Faculty of Advanced Technology and Multidiscipline, Airlangga University, Surabaya, Indonesia

ABSTRACT

A new highly water stable bismuth-containing coordination polymer is reported along with its structural characterizations as determined by single crystal and powder X-ray diffraction, elemental, and thermal analysis, featuring an orange-red photoluminescence, and proton conductivity. The compound, $(Imi)_2[Bi_2(pzdc)_4]\cdot 2H_2O$ (**1**, $pzdc^{2-}$ = pyrazine-2,3-dicarboxylate; Imi = imidazolium cation), crystallizes in the monoclinic space group, $P2_1/c$ ($a = 14.3725(7)$ Å, $b = 22.4499(10)$ Å, $c = 11.5204(6)$ Å, and $\beta = 91.1183(16)^\circ$), which contains 2D layers of Bi that are connected into a 3D supramolecular structure via extended hydrogen bond network. The interlayered voids are occupied by lattice water and imidazolium ions. Compound **1** is synthesized using an optimized, facile slow evaporation method leading to a water stable compound with a well-defined 1D hydrogen-bonded water feature along the crystallographic *a*-direction that lead to a proton conductivity of 8.41×10^{-6} S·cm^{-1} at 85 °C and 95% RH.

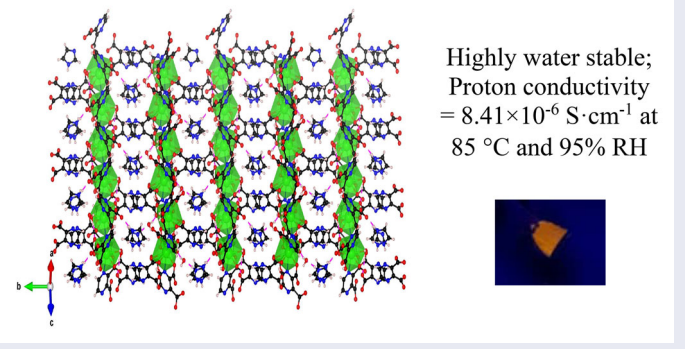

ARTICLE HISTORY
Received 31 January 2021
Accepted 15 April 2021

KEYWORDS
Bismuth coordination polymer; pyrazine-2,3-dicarboxylic acid; water stable; photoluminescence; proton conductivity

CONTACT Arief C. Wibowo wibowor@gmail.com Faculty of Advanced Technology and Multidiscipline, Airlangga University, Surabaya 60115, Indonesia

Supplemental data for this article is available online at https://doi.org/10.1080/00958972.2021.1921167.

1. Introduction

Crystalline materials, especially metal-organic coordination polymers (MOCPs) built from self-assembly of metal ions and organic ligands, have been investigated in the field of proton conduction [1–7]. Distinct from other conventional proton conducting materials, such as Nafion [8, 9] or polymers [10, 11], a well-defined structure and crystallinity in MOCPs permit accurate identification of relevant structural information crucial for understanding the proton-conduction routes and other mechanisms involved. However, the lability of metal-ligand bonds in most MOCPs, linked to the mismatch between the Lewis acid-base pairs based on the concept of Hard-Soft Acid-Base (HSAB) principle [12], limits their applications especially in the presence of moisture, variable pH, or high temperatures [13–15]. Stability for the required temperature range, pH, and in the presence of water is essential for practical use of MOCP-based proton conduction applications [16, 17]. Further, facile transport of charge through the proton conductor is a prerequisite to effective ion conduction. An efficient ion conduction in MOCPs occurs via transport pathway of sites of similar proton affinity separated by a minimum energy barrier [17]. Arrays of proton carriers which gave rise to proton conduction pathways in MOCPs are typically introduced by grafting acidic groups onto the framework backbones [18, 19] or via encapsulation of guest molecules such as imidazole, ammonium ions, or volatile acids [20]. Imidazole molecules are often incorporated to enhance the proton conductivities of crystalline and other porous materials, especially in the so-called water assisted proton-conducting MOCPs which rely on the presence of water molecules or hydrogen-bonding interactions with water molecules [21, 22]. Incorporated imidazole molecules improve the proton conductivity by increasing the concentration of protons in the materials. However, the exact spatial arrangements of imidazole molecules and how they enhance the overall acidity and hydrophilicity are not always clear [23].

In our quest to synthesize water stable MOCP, we opt for borderline Bi^{3+} cation and multidentate pyrazine-2,3-dicarboxylic acid (H_2pzdc) with six potential donor atoms, including soft N-donors of the pyrazine ring and hard O-donors of the carboxylate group that are expected to lead to the construction of a highly stable and ordered framework with Bi^{3+}. The presence of N-donor ligands in the coordination sphere of borderline or soft cations increases the thermodynamic stability of the framework due to strong metal–N interaction leading to high bond dissociation energy [12, 24]. In addition to this, H_2pzdc also enables formation of highly hydrophilic materials that can bind water selectively, owing to its back-donation feature [25]. In addition, both Bi^{3+} [26–31] and $pzdc^{2-}$ [32] based MOCPs have been of interest, owing to their potential use for optically related applications.

Herein, we report a new, highly stable Bi^{3+}-based 2D MOCP, $(Imi)_2[Bi_2(pzdc)_4]\cdot 2H_2O$ (**1**, $pzdc^{2-}$ = pyrazine-2,3-dicarboxylate, Imi = imidazolium cations) synthesized using a simple, low temperature dissolution-slow evaporation method, featuring high water stability, 1D hydrogen-bonded lattice water and imidazolium ions along the *a*-direction that leads to proton conductivity of 8.41×10^{-6} S·cm^{-1} at 85 °C and 95% RH. Its optimized synthetic condition, structural, thermal, and photophysical characterizations and water stability, as well as proton conductivity, are presented.

Table 1. Crystal data and structure refinement of 1.[a]

Empirical formula	$C_{30}H_{22}Bi_2N_{12}O_{18}$
Formula weight	1256.55
Temperature	100(2) K
Wavelength	0.71073 Å
Crystal system	Monoclinic
Space group	$P\ 2_1/c$
Unit cell dimensions	$a = 14.3725(7)$ Å $b = 22.4499(10)$ Å $c = 11.5204(6)$ Å $\alpha = 90°$ $\beta = 91.1183(16)°$ $\gamma = 90°$
Volume	3716.5(3) Å^3
Z	4
Density (calculated)	2.246 g/cm^3
Absorption coefficient	9.555 mm^{-1}
F(000)	2384
Crystal size	0.175 × 0.051 × 0.034 mm^3
θ Range for data collection	2.30 to 28.35°
Index ranges	$-19<=h<=19$, $-29<=k<=29$, $-15<=l<=15$
Reflections collected	115677
Independent reflections	9267 [$R_{int} = 0.0$]
Completeness to $\theta = 28.35°$	99.3%
Refinement method	Full-matrix least-squares on F^2
Data / restraints / parameters	9267 / 6 / 571
Goodness-of-fit	1.102
Final R indices [$I > 2\sigma(I)$]	$R_{obs} = 0.0229$, $wR_{obs} = 0.0438$
R indices [all data]	$R_{all} = 0.0297$, $wR_{all} = 0.0454$
Largest diff. peak and hole	1.501 and −2.461 e·Å^{-3}

[a] $R = \sum ||F_0| - |F_C|| / \sum |F_0|$. $wR_2 = \{\sum[w(F_0^2 - F_C^2)^2] / \sum[w(F_0^2)^2]\}^{1/2}$.

2. Results and discussion

Compound **1** was synthesized via a simple and facile slow evaporation reaction between $Bi(NO_3)_3{\cdot}5H_2O$ and H_2pzdc in DMF/H_2O (1:1) mixed solvents, in the presence of imidazole, under optimized conditions. Single-crystal X-ray diffraction analysis reveals that colorless plate crystals of **1** crystallize in the monoclinic $P2_1/c$ space group with $a = 14.3725(7)$ Å, $b = 22.4499(10)$ Å, $c = 11.5204(6)$ Å, and $\beta = 91.1183(16)°$. Relevant crystallographic data from the single-crystal structure refinement are found in Table 1. Selected interatomic distances and angles are summarized in Table 2. The asymmetric unit of **1** contained two Bi^{3+} ions, four equivalent $pzdc^{2-}$ molecules, two lattice water molecules, and two lattice imidazolium ions (Figure 1(a)). Each Bi^{3+} is nine-coordinate, surrounded by seven oxygen and two nitrogen donors from five $pzdc^{2-}$ ligands completing the coordination sphere, giving a distorted bicapped pentagonal bipyramid of ($Bi(1)N_2O_7$) and ($Bi(2)N_2O_7$) (Figure 1(b)). All the Bi^{3+} polyhedra are holodirected containing stereochemically inactive lone pairs (Figure 1(b)). The $pzdc^{2-}$ ligands in this compound adopt different coordination modes, e.g. *O,O*-chelation, monodentate, as well as *N,O*-chelation, including uncoordinated oxygen atoms (Supporting Information Figure S1).

The whole structure of **1** is composed of Bi(1) and Bi(2) chains which are bridged by $pzdc^{2-}$ ligands in an *N,O*-chelation mode via O5, N3, and O7, N4 forming a 2D layer along the *ac* plane (Figure 2(a)). Each Bi(1) center is connected to another Bi(1) through $pzdc^{2-}$ ligand in a chelation mode through O1, O2 and O3, O4, and another

Table 2. Representative bond lengths (Å) and angles (°) for 1.[a]

Label	Distances/Angles
Bi(1)-O(5)	2.321(2)
Bi(1)-O(3)	2.327(2)
Bi(1)-O(16)#1	2.427(3)
Bi(1)-O(1)#2	2.514(3)
Bi(1)-O(2)#2	2.716(3)
Bi(1)-O(6)#2	2.629(3)
Bi(1)-O(4)	2.800(3)
Bi(1)-N(8)#1	2.512(3)
Bi(1)-N(3)	2.567(3)
Bi(2)-O(13)	2.333(2)
Bi(2)-O(9)	2.354(3)
Bi(2)-O(7)	2.374(2)
Bi(2)-O(11)#3	2.523(3)
Bi(2)-O(14)#3	2.622(2)
Bi(2)-O(12)#3	2.710(3)
Bi(2)-O(10)	2.756(3)
Bi(2)-N(4)	2.527(3)
Bi(2)-N(7)	2.562(3)
O(2)-C(5)	1.247(5)
O(1)-C(5)	1.265(4)
O(4)-C(6)	1.242(4)
C(1)-N(1)	1.344(5)
C(2)-N(2)	1.337(5)
C(3)-N(2)	1.332(5)
C(4)-N(1)	1.334(5)
O(5)-Bi(1)-O(3)	77.10(9)
O(5)-Bi(1)-O(16)#1	142.09(9)
O(5)-Bi(1)-N(8)#1	75.98(9)
O(3)-Bi(1)-N(8)#1	69.61(9)
O(5)-Bi(1)-O(1)#2	77.45(9)
O(16)#1-Bi(1)-N(3)	139.78(9)
O(1)#2-Bi(1)-N(3)	124.35(9)
N(8)#1-Bi(1)-N(3)	133.34(9)
O(3)-Bi(1)-O(2)#2	148.78.(9)
O(13)-Bi(2)-O(7)	140.76(9)
O(9)-Bi(2)-O(7)	83.74(9)
O(13)-Bi(2)-O(11)#3	78.85(9)
O(9)-Bi(2)-O(11)#3	136.76(9)
O(7)-Bi(2)-O(11)#3	92.93(9)
O(13)-Bi(2)-N(4)	74.44(9)
O(9)-Bi(2)-N(4)	70.25(9)
O(7)-Bi(2)-N(4)	66.89(9)
O(11)#3-Bi(2)-N(4)	68.90(9)
O(13)-Bi(2)-N(7)	66.81(9)
O(7)-Bi(2)-N(7)	141.53(9)

[a]Symmetry transformations used to generate equivalent atoms: (1) $x - 1, y, z$ (2) $x, -y + 1/2, z + 1/2$ (3) $x, -y + 1/2, z - 1/2$ (4) $x + 1, y, z$.

$pzdc^{2-}$ further connects the adjacent Bi(1) center via N3, O5, and O6 in an *N,O*-chelation and monodentate O, leading to a 1D chain of Bi(1) along the *c*-axis (Supporting Information Figure S2(a)). Similar connections are also observed between Bi(2) centers via chelation mode (O9, O10 and O11, O12) of the same $pzdc^{2-}$ ligand, and *N,O*-chelation mode as well as monodentate modes (N3, O13, and O14) of another $pzdc^{2-}$ ligand, also leading to Bi(2) chains along the *c*-axis (Supporting Information Figure S2(b)).

Along the *a*-axis, two lattice water molecules (H17W and H18W) are hydrogen bonded to the coordinated carboxylate O (O1, O2, O11, and O12) arranged pointing to outer sides of the 2D layers forming a network of hydrogen bonds on top and

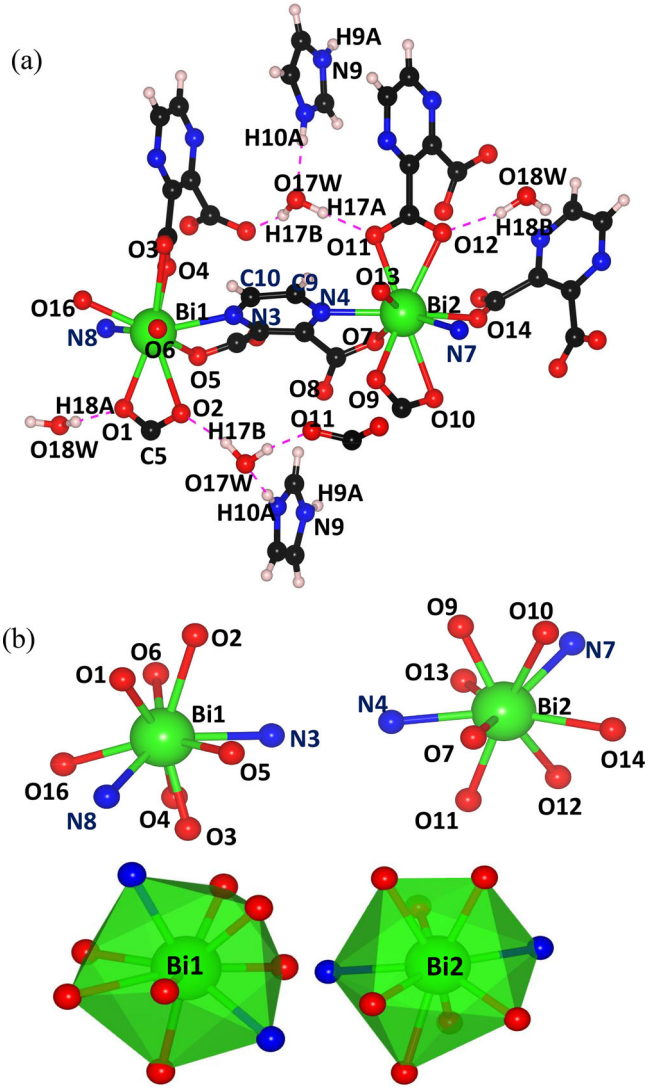

Figure 1. (a) Asymmetric unit and atomic labeling of **1**. (b) The holo-directed bismuth centered polyhedra of $Bi(1)O_7N_2$ and $Bi(2)O_7N_2$.

below the 2D layers (Supporting Information Figure S3). The oxygen of lattice water (O17W) is also hydrogen bonded to the H10A of the imidazolium ion further pointing outside the 2D layer (Supporting Information Figure S3(b)). Free uncoordinated carboxylate O (O15) is also hydrogen bonded with another imidazolium ion (Supporting Information Figure S3(b)).

Neighboring 2D layers are connected through hydrogen bonding between the imidazolium ions and N2/O4 of the $pzdc^{2-}$ ligand along the *b*-axis (Figure 2(c) and Supporting Information Figure S3), forming a 3D supramolecular framework with interlayered voids filled with hydrogen bonded imidazolium ions and lattice water molecules (Figure 2(d) and Supporting Information Figure S3). Bi–O bond distances range

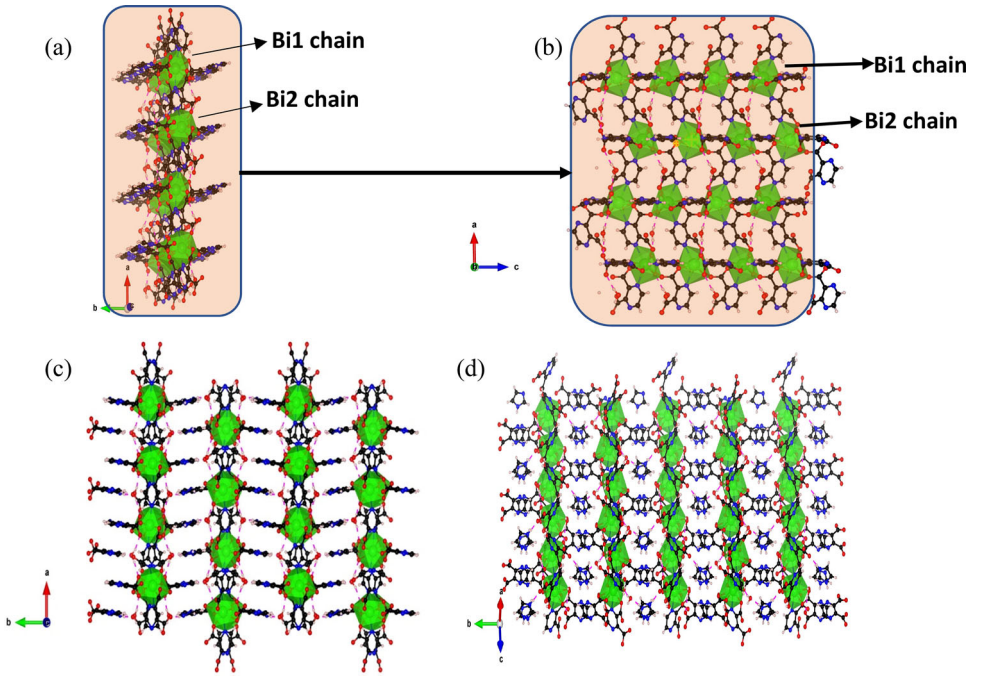

Figure 2. (a) A single 2D layer viewed along the *ac*-plane; (b) a 2D layer showing alternating Bi(1) and Bi(2) chains along the *a*-axis; (c) 3D supramolecular framework of **1** with network of H-bonds connecting the neighboring 2D layers; (d) 3D supramolecular structure with interlayer voids filled with H-bonded imidazolium ions and lattice water molecules.

from 2.321(2)–2.800(3) Å, and Bi–N bond distances range from 2.512(3) to 2.567(3) Å, typical of Bi^{3+}- based compounds [27, 30, 33–41].

Crystallinity and phase purity indicating the presence or absence of polymorphs can be detected by powder X-ray diffraction (PXRD). The purity of **1**, plate crystals, was checked using PXRD. The powder diffraction patterns of **1** matched exactly with the calculated patterns of the single crystal structural data as shown in Figure 3, demonstrating that within the resolution and detection limit of PXRD, the reaction products used for further physical characterizations are of single phase, and no additional polymorph is present or unreacted starting material remains in the samples. The morphology of the bulk crystals shows plate-like crystals as shown in optical image, with the corresponding white color (Supporting Information Figure S4).

2.1. Water stability

Realizing that the structure has a fully 2D coordination framework, featuring also an extended hydrogen-bonded lattice water and imidazolium ions between the 2D layers, it then becomes imperative to check the water stability of **1**. The stability was tested by soaking it in water for 2 months at room temperature as well as refluxing in water for 1 day. Interestingly, the structure is still maintained after soaking for 2 months and 1 d reflux; in both patterns, there is no indication of product decomposition and the

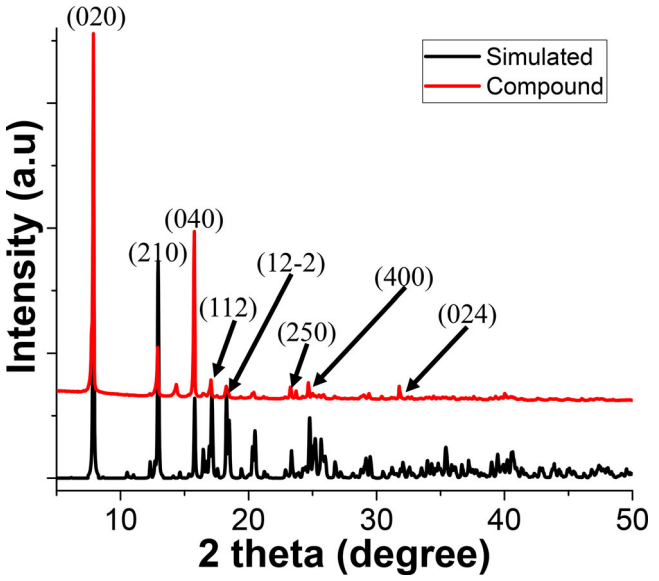

Figure 3. PXRD patterns of **1** showing simulated (bottom) *vs*. observed (top).

crystallinity is well preserved, which shows the robustness of **1** (Supporting Information Figure S5).

Thermogravimetric analysis (TGA) under N_2 also shows that **1** has thermal stability up to 350 °C (Supporting Information Figure S6). The TGA thermogram shows an initial weight loss of 2.85% between 120 °C and 350 °C, agreeing well with calculated initial weight loss of 2.87%, which correspond to two lattice water molecules per formula unit. The thermogram shows a further weight loss of 53.81% between 350 °C and 450 °C, equivalent to the loss of four $pzdc^{2-}$ ligands which also agrees well with single crystal data refinement with calculated value of 52.87%. These results agree well with the CHN elemental analysis, confirming the formula obtained from crystallography.

2.2. Evaluation of photoluminescence emission

Room temperature solid state emission of **1** including its optical image representing its photoluminescence (PL) color emission is shown in Figure 4. When excited at 350 nm, **1** emits an orange-red color with an emission maximum at 635 nm. Free H_2pzdc has no apparent PL in the solid state at room temperature [42, 43]; the emission may be attributed to ligand-to-metal charge transfer (LMCT) as supported by UV–Vis spectral analysis of **1** which shows disappearance of the peak at 260 nm in H_2pzdc compared to **1**. Observation of LMCT is further indicated by the red-shift of the ligand's 320 nm band to approximately 350 nm in **1** (Supporting Information Figure S7). Such electronic transitions are commonly observed in Bi-based coordination polymers [26, 28].

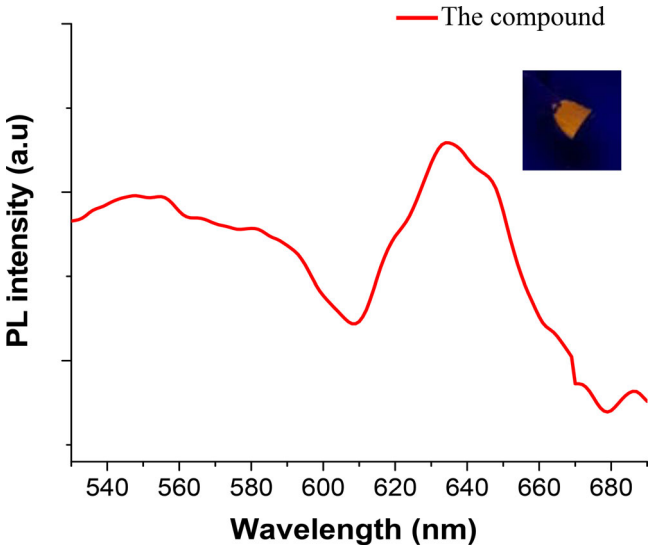

Figure 4. Solid state PL emission of **1** excited at 350 nm with an insert showing its digital image under a 365 nm UV lamp.

2.3. Proton conductivity

The presence of extended, hydrogen-bonded lattice water and imidazolium ions along the *a*-direction may attract more dynamic lattice water into the interlayer void space. This and the fact that the resulting compound is highly stable after 2 months of soaking and 1 day reflux in water, fulfill the general pre-requisite for proton conductivity [44, 45]. Alternating current impedance analysis with controlled relative humidity (RH) and temperature was used to measure proton conductivity of **1** using a pelletized sample and the resulting conductivities were calculated from fitting of the Nyquist plots (Figure 5(a)), while the corresponding Arrhenius plot of **1** is shown in Supporting Information Figure S8. The activation energy for the proton transfer is calculated as 0.31 eV (Supporting Information Figure S8), which is in the higher end of that generally regarded for a Grotthuss mechanism, i.e. a less efficient proton hopping mechanism. As shown in Supporting Information Table S1, the room temperature conductivity increases with increasing of RH with highest value at 95% RH. A cycle of heating and cooling at 95% RH results in the highest proton conductivity of 8.41×10^{-6} S·cm^{-1}, at 85 °C and 95% RH (Supporting Information Table S2). Table 3 compares the proton conductivity of some reported MOCPs with the current work, placing **1** among the best [23, 46–49]. Post measurement PXRD (Post PC), Figure 5(b), shows that the PXRD of the original phase is maintained with no additional phase after proton conductivity measurements (Post PC), suggesting that the integrity of the structure is well preserved.

The moderate proton conduction can be explained by considering the single crystal structure. The presence of well-ordered guests enables structural determination, but at the same time may imply lower mobility. Further, in **1**, the proton conduction channels only propagate in one dimension (Supporting Information Figure S9), meaning

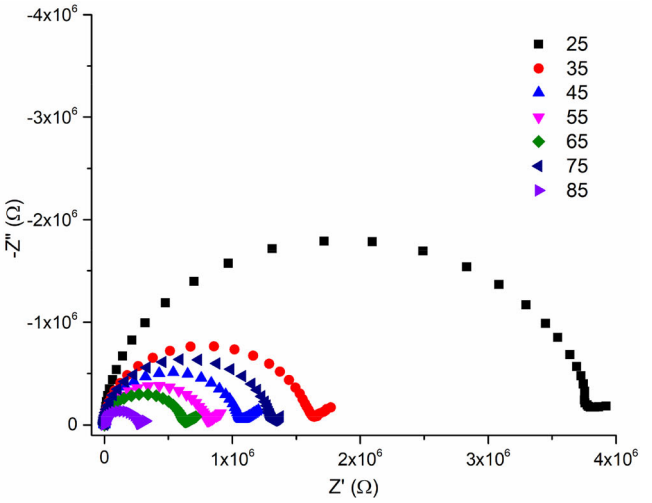

(a)

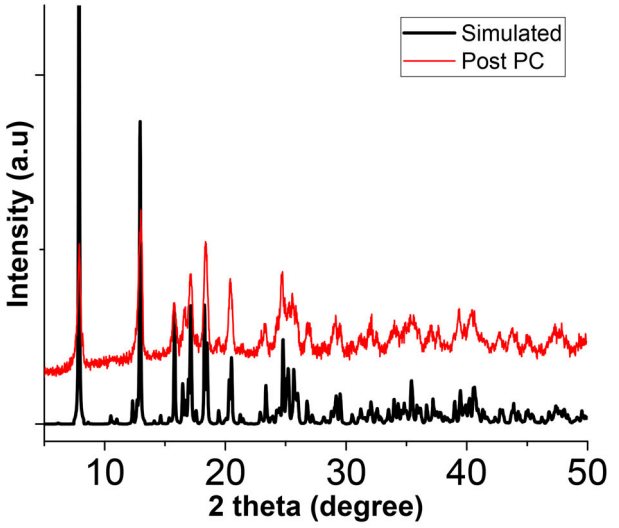

(b)

Figure 5. (a) Nyquist plot of **1** at 95% RH with varied temperatures; (b) PXRD pattern of **1** after proton conductivity (Post PC) measurements: Simulated (bottom) *vs*. Post PC (top).

that multidirectional efficient transport is a challenge and consequently, grain boundary resistances would be enhanced [50]. Although the proton conductivity is of moderate value for proton conducting MOCPs [44, 45], its high water stability and the fact that lone-pair containing compounds are adaptable to defects [51–54], the proton or ionic conductivity of **1** may be increased by cation exchange with highly mobile ions or incorporating a highly mobile guest cation that facilitates ion conductivity.

Table 3. Proton conductivity of some MOCPs *vs*. current work.

MOCPs	Temp. (°C)	% RH	Conductivity ($S \cdot cm^{-1}$)	Ref.
$(Imi)_2[Bi_2(pzdc)_4]\cdot 2H_2O$	85	95	8.41×10^{-6}	This work
Fe-MOF	60	98	1.25×10^{-4}	[23]
Im@Fe-MOF	60	98	4.23×10^{-3}	[23]
Im-Fe-MOF	60	98	1.21×10^{-2}	[23]
Ni(BDC)@Imidazole	90	Anhydrous	6.04×10^{-5}	[46]
$Imi@[Al(\mu_2\text{-}OH)(1,4\text{-}ndc)]_n$	RT	Anhydrous	5.50×10^{-8}	[47]
$Imi@[Al(\mu_2\text{-}OH)(1,4\text{-}ndc)]_n$	120	Anhydrous	2.20×10^{-5}	[47]
$Imi@[Al(\mu_2\text{-}OH)(1,4\text{-}bdc)]_n$	120	Anhydrous	1.00×10^{-7}	[47]
Imi@UiO-67	120	Anhydrous	1.44×10^{-3}	[48]
$\{[(Me_2NH_2)_3(SO_4)]_2[Zn_2(ox)_3]\}_n$	150	Anhydrous	1.00×10^{-4}	[49]
$\{[(Me_2NH_2)_3(SO_4)]_2[Zn_2(ox)_3]\}_n$	150	98	1.00×10^{-4}	[49]

3. Experimental

3.1. Materials and methods

All chemicals were of reagent grade and used without purification. $Bi(NO_3)_3\cdot 5H_2O$, pyrazine-2,3-dicarboxylic acid, and imidazole were purchased from Sigma-Aldrich. Thermogravimetric analysis (TGA) was recorded on a Perkin Elmer TGA 6 Thermogravimetric analyzer under air using 5 °C/min heating rate. Elemental analyses were performed using a Perkin Elmer CHNS/O 2400 Series II. Solid state UV–Vis spectra were recorded on a UV–Vis-NIR Lambda 950. Solid state photoluminescence measurements were performed using a FLS920, Edinburgh Instrument with steady-state time resolved PL measurement capability.

3.2. Synthesis of $(Imi)_2[Bi_2(pzdc)_4]\cdot 2H_2O$ (1)

A mixture of $Bi(NO_3)_3\cdot 5H_2O$ (0.1213 g, 0.25 mmol), pyrazine-2,3-dicarboxylic acid (H_2pzdc) (0.1009 g, 0.30 mmol) and imidazole (0.0204 g, 0.30 mmol) was dissolved in a 20 mL mixture of DMF:H_2O 1:1 ratio while heating at 48 °C and stirring for approximately 10 min. After filtration, the filtrate was left for slow evaporation. Plate crystals with nearly quantitative yield were formed after 4 days. The final product was washed thoroughly with fresh DI water, isolated by vacuum filtration, and dried at room temperature. A quantitative elemental analysis calculated for **1**, ($C_{30}H_{22}Bi_2N_{12}O_{18}$): C, 28.67; H, 1.76; N, 13.63%; and the CHN elemental analysis found for **1**d, C, 28.55; H, 1.49; and N, 13.25%.

3.3. X-ray crystallography

X-ray intensity data from a colorless plate of **1** were measured at 100(2) K using a Bruker D8 QUEST diffractometer (Mo Kα radiation, $\lambda = 0.71073$ Å). Direct methods structure solution, difference Fourier calculations and full-matrix least-squares refinement against F^2 were performed with SHELXTL [55]. Hydrogens of the ligand were placed in geometrically idealized positions and included as riding atoms. The water hydrogens ($x = 0.7$) were located in difference maps and refined isotropically with their O-H distances restrained to be similar.

3.4. Powder X-ray diffraction

Ground mixtures of single crystals of the samples were used to collect powder X-ray diffraction patterns using a PanAlytical X'Pert Pro Powder Diffractometer (Cu Kα radiation $\lambda = 1.5418$ Å) over the 2θ range of $5 - 50^{\circ}$, with a step size of 0.02° and a scan speed of 0.25°/min. The measured patterns were compared to the simulated diffraction patterns using the single crystal data.

3.5. Proton conductivity measurement

Electrochemical impedance measurements were performed on a Princeton Applied Research VersaSTAT3 potentiostat/galvanostat with environment maintained by an E-Spec BTL-433 humidity-controlled oven. Experiments were performed in air, at 25 °C and 85 °C while humidity levels maintained at 95% relative humidity (RH), after a full cycle of RH variation (from 35% to 95%) at constant 25 °C. The samples were finely ground to a powder by mortar and pestle prior to loading in custom dual-sample 2-probe cells with titanium electrodes. Electrodes were hand tightened, then tightened to an unknown pressure (with a screwdriver) to ensure good contact. Cell (sample) lengths were between 0.15 and 0.3 cm, with a 0.317 cm diameter. At a minimum two full heating/cooling cycles were performed with a minimum of 24 h between temperature points. Duplicate measurements were obtained sweeping from 1 MHz to 0.1 Hz and then in reverse. Data were collected using VersaStudio software (version 2.1). ZView Software was used to fit impedance data sets by simulating an equivalent circuit.

4. Conclusion

We synthesized a new and highly water stable 2D Bi MOCP by combining pyrazine-2,3-dicarboxylic acid ligand and Bi^{3+} using a simple and facile slow evaporation method with addition of imidazole required to obtain a nearly quantitative yield. Compound **1** featured a 2D layered structure connected by extensive 1D hydrogen bonding due to the presence of lattice water and imidazolium ions in the interlayer to give a 3D supramolecular structure. Solid state PL analysis shows that when excited at 350 nm, **1** emits orange-red color with a broad peak at 635 nm. Compound **1** further shows a moderate proton conductivity of 8.41×10^{-6} S·cm^{-1} at 85 °C and 95% RH due to an extended hydrogen-bonded lattice water feature along the crystallographic *a*-direction.

Disclosure statement

No potential conflict of interest was reported by the authors.

Data availability

Crystallographic data for the structures reported in this paper have been deposited with the Cambridge Crystallographic Data Center as supplementary publication no. CCDC 2032173 for **1**. These data can be obtained free of charge via www.ccdc.cam.ac.uk/data_request/cif, by emailing

data_request@ccdc.cam.ac.uk, or by contacting the Cambridge Crystallographic Data Center, 12 Union Road, Cambridge CB21EZ, UK; Fax: +44 1223 336033.

Funding

This work was supported by [HIR Chancellory Grant] under [UM.C/625/1/HIR/211] from the University of Malaya; [FRGS, Ministry of Education, Malaysia,] Project [No. FP 037-2014A]. K.M.O. acknowledges the financial support from the National Research Foundation of Korea funded by the Ministry of Science and ICT (Grant Nos. 2018R1A5A1025208 and 2019R1A2C3005530).

References

[1] Y. Cao, X. Zhou, L. Luan, H. Zeng, G. Zou, Z. Lin. *Z. Lin. Inorg. Chem. Commun.*, **124**, 108403 (2021).
[2] S. Chand, S.C. Pal, D.-W. Lim, K. Otsubo, A. Pal, H. Kitagawa, M.C. Das. *ACS Mater. Lett.*, **2**, 1343 (2020).
[3] L. Huang, L. Wang, Y. Zhao, L. Huang, J. Bi, G. Zou, Z. Lin, D. Gao. *Dalton Trans.*, **49**, 5440 (2020).
[4] A. Mohanty, U.P. Singh, A. Ghorai, S. Banerjee, R. Butcher. *Cryst. Eng. Comm.,* **23**, 684 (2021).
[5] Z. Que, Y. Ye, Y. Yang, F. Xiang, S. Chen, J. Huang, Y. Li, C. Liu, S. Xiang, Z. Zhang. *Inorg. Chem.*, **59**, 3518 (2020).
[6] X.-Y. Zeng, Y.-L. Wang, Z.-T. Lin, Q.-Y. Liu. *Inorg. Chem.*, **59**, 12314 (2020).
[7] Y. Zhang, H. Jiang, L. Luan, H. Zeng, G. Zou, Z. Lin. *Z. Lin. J. Solid State Chem.*, **292**, 121709 (2020).
[8] X. Yang, H. Zhu, F. Jiang, X. Zhou. *J. Power Sources*, **473**, 228586 (2020).
[9] M.B. Karimi, F. Mohammadi, K. Hooshyari. *J. Membr. Sci.*, **605**, 118116 (2020).
[10] K.-D. Kreuer. *Chem. Mater.*, **26**, 361 (2014).
[11] W. You, K.J. Noonan, G.W. Coates. *Prog. Polym. Sci.*, **100**, 101177 (2020).
[12] A.M. Hamisu, A. Ariffin, A.C. Wibowo. *Inorg. Chim. Acta*, **511**, 119801 (2020).
[13] H. Li, M. Eddaoudi, M. O'Keeffe, O.M. Yaghi. *Nature*, **402**, 276 (1999).
[14] N. Al-Janabi, P. Hill, L. Torrente-Murciano, A. Garforth, P. Gorgojo, F. Siperstein, X. Fan. *Chem. Eng. J.*, **281**, 669 (2015).
[15] X. Zhang, B. Wang, A. Alsalme, S. Xiang, Z. Zhang, B. Chen. *Coord. Chem. Rev.*, **423**, 213507 (2020).
[16] J.M. Taylor, K.W. Dawson, G.K. Shimizu. *J. Am. Chem. Soc.*, **135**, 1193 (2013).
[17] G.K. Shimizu, J.M. Taylor, S. Kim. *Science*, **341**, 354 (2013).
[18] F. Yang, H. Huang, X. Wang, F. Li, Y. Gong, C. Zhong, J.-R. Li. *Cryst. Growth Des.*, **15**, 5827 (2015).
[19] W.J. Phang, H. Jo, W.R. Lee, J.H. Song, K. Yoo, B. Kim, C.S. Hong. *Angew. Chem.*, **127**, 5231 (2015).
[20] S.-J. Liu, C. Cao, F. Yang, M.-H. Yu, S.-L. Yao, T.-F. Zheng, W.-W. He, H.-X. Zhao, T.-L. Hu, X.-H. Bu. *Cryst. Growth Des.*, **16**, 6776 (2016).
[21] A. Shigematsu, T. Yamada, H. Kitagawa. *J. Am. Chem. Soc.*, **133**, 2034 (2011).
[22] M. Bazaga-García, R.M.P. Colodrero, M. Papadaki, P. Garczarek, J. Zoń, P. Olivera-Pastor, E.R. Losilla, L. León-Reina, M.A.G. Aranda, D. Choquesillo-Lazarte, K.D. Demadis, A. Cabeza. *J. Am. Chem. Soc.*, **136**, 5731 (2014).
[23] F.-M. Zhang, L.-Z. Dong, J.-S. Qin, W. Guan, J. Liu, S.-L. Li, M. Lu, Y.-Q. Lan, Z.-M. Su, H.-C. Zhou. *J. Am. Chem. Soc.*, **139**, 6183 (2017).
[24] M. Bosch, M. Zhang, H.-C. Zhou. *Adv. Chem.*, **2014**, 1(2014).
[25] M. Lankelma, J. de Boer, M. Ferbinteanu, A.L.D. Ramos, R. Tanasa, G. Rothenberg, S. Tanase. *Dalton Trans.*, **44**, 11380 (2015).

[26] A.C. Wibowo, M.D. Smith, H.-C. Zur Loye. *Cryst. Growth Des.*, **11**, 4449 (2011).
[27] A.C. Wibowo, M.D. Smith, H.-C. Zur Loye. *Chem. Commun. (Camb))*, **47**, 7371 (2011).
[28] A.C. Wibowo, S.A. Vaughn, M.D. Smith, H.-C. Zur Loye. *Inorg. Chem.*, **49**, 11001 (2010).
[29] T. Rhauderwiek, C. dos Santos Cunha, H. Terraschke, N. Stock. *Eur. J. Inorg. Chem.*, **2018**, 3232(2018).
[30] B.J. Deibert, E. Velasco, W. Liu, S.J. Teat, W.P. Lustig, J. Li. *J. Li. Cryst. Growth Des.*, **16**, 4178 (2016).
[31] A.K. Adcock, B. Gibbons, J.D. Einkauf, J.A. Bertke, J.F. Rubinson, D.T. de Lill, K.E. Knope. *Dalton Trans.*, **47**, 13419 (2018).
[32] A.M. Hamisu, F.Y. Wardana, A. Ariffin, I. Baig, C.D. Malliakas, A.C. Wibowo. *J. Solid State Chem.*, **279**, 120948 (2019).
[33] B. Li, H. Zhang, L. Huynh, C. Diverchy, S. Hermans, M. Devillers, E.V. Dikarev. *Inorg. Chem.*, **48**, 6152 (2009).
[34] A.S. Filatov, M. Napier, V.D. Vreshch, N.J. Sumner, E.V. Dikarev, M.A. Petrukhina. *Inorg. Chem.*, **51**, 566 (2012).
[35] E.V. Dikarev, B. Li. *Inorg. Chem.*, **43**, 3461 (2004).
[36] E.V. Dikarev, T.G. Gray, B. Li. *Angew. Chem. Int. Ed. Engl.*, **44**, 1721 (2005).
[37] G. Wang, Q. Sun, Y. Liu, B. Huang, Y. Dai, X. Zhang, X. Qin. *Chemistry*, **21**, 2364 (2015).
[38] G. Wang, Y. Liu, B. Huang, X. Qin, X. Zhang, Y. Dai. *Dalton Trans.*, **44**, 16238 (2015).
[39] Y.-Q. Sun, S.-Z. Ge, Q. Liu, J.-C. Zhong, Y.-P. Chen. *CrystEngComm*, **15**, 10188 (2013).
[40] M. Savage, S. Yang, M. Suyetin, E. Bichoutskaia, W. Lewis, A.J. Blake, S.A. Barnett, M. Schröder. *Chemistry*, **20**, 8024 (2014).
[41] M. Feyand, E. Mugnaioli, F. Vermoortele, B. Bueken, J.M. Dieterich, T. Reimer, U. Kolb, D. de Vos, N. Stock. *Angew. Chem. Int. Ed. Engl.*, **51**, 10373 (2012).
[42] H. Yin, S.-X. Liu. *Polyhedron*, **26**, 3103 (2007).
[43] Y. Ma, Z. Han, Y. He, P. Zhao. *J. Coord. Chem.*, **61**, 563 (2008).
[44] P. Ramaswamy, N.E. Wong, G.K.H. Shimizu. *Chem. Soc. Rev.*, **43**, 5913 (2014).
[45] S. Horike, D. Umeyama, S. Kitagawa. *Acc. Chem. Res.*, **46**, 2376 (2013).
[46] Z. Bai, S. Liu, P. Chen, G. Cheng, G. Wu, Y. Liu. *Nanotechnology*, **31**, 125702 (2020).
[47] S. Bureekaew, S. Horike, M. Higuchi, M. Mizuno, T. Kawamura, D. Tanaka, N. Yanai, S. Kitagawa. In *Materials for Sustainable Energy: A Collection of Peer-Reviewed Research and Review Articles from Nature Publishing Group*, pp. 232–237, UK (2011).
[48] S. Liu, Z. Yue, Y. Liu. *Dalton Trans.*, **44**, 12976 (2015).
[49] S.S. Nagarkar, S.M. Unni, A. Sharma, S. Kurungot, S.K. Ghosh. *Angew. Chem. Int. Ed. Engl.*, **53**, 2638 (2014).
[50] N.E. Wong, P. Ramaswamy, A.S. Lee, B.S. Gelfand, K.J. Bladek, J.M. Taylor, D.M. Spasyuk, G.K.H. Shimizu. *J. Am. Chem. Soc.*, **139**, 14676 (2017).
[51] G. Laurita, D.H. Fabini, C.C. Stoumpos, M.G. Kanatzidis, R. Seshadri. *Chem. Sci.*, **8**, 5628 (2017).
[52] D.H. Fabini, J.G. Labram, A.J. Lehner, J.S. Bechtel, H.A. Evans, A. Van der Ven, F. Wudl, M.L. Chabinyc, R. Seshadri. *Inorg. Chem.*, **56**, 11 (2017).
[53] C.K. Brozek, M. Dincă. *Chem. Soc. Rev.*, **43**, 5456 (2014).
[54] R.E. Brandt, J.R. Poindexter, P. Gorai, R.C. Kurchin, R.L.Z. Hoye, L. Nienhaus, M.W.B. Wilson, J.A. Polizzotti, R. Sereika, R. Žaltauskas, L.C. Lee, J.L. MacManus-Driscoll, M. Bawendi, V. Stevanović, T. Buonassisi. *Chem. Mater.*, **29**, 4667(2017).
[55] G.M. Sheldrick. *SHELXTL Ver. 6.14 Edn.*, Bruker Analytical X-Ray Systems, Inc., Madison, Wisconsin (2003).